Microchimica Acta (2021) 188: 389
https://doi.org/10.1007/s00604-021-05048-w

ORIGINAL PAPER

In situ growth of electroactive polymers via ATRP to construct a biosensing interface for tumor marker

Fei Wang[1] · Yang Xu[1] · Hongliang Han[1] · Zhanfang Ma[1]

Received: 10 June 2021 / Accepted: 4 October 2021 / Published online: 22 October 2021

Abstract

A novel biosensing interface for tumor markers was designed based on the atom transfer radical polymerization (ATRP) of poly(isopropenylphenol) (PPPL) in situ initiated by the fixing of p-chloromethyl benzoic acid on the surface of amino-modified electrodes. It was found that the electrochemical activity of PPPL itself can provide sufficient signals for these biosensors, which can avoid signal leakage and streamline the interface modification process. Cu(II) ions absorbed on the carbon spheres and then were released via acid stimulation to act as a catalyst to participate in the interface polymerization with ATRP. As the concentration of targets increased, more Cu(II) ions were released, and the electrochemical signal of polymers was enhanced. Therefore, the sensitive detection of carbohydrate antigen 19–9 (CA19-9) as a model target was achieved, with an ultralow limit of detection of 39 μU mL^{-1} and wide detection range from 100 μU mL^{-1} to 100 U mL^{-1} under optimal conditions. Furthermore, this method achieved satisfying performance in human blood serum with good inter-assay precision ($RSD < 6\%$) and satisfactory recovery of ~ 99–105%. According to the results, this work is of great significance for constructing biosensor interfaces via in situ polymerization.

Keywords Electrochemical biosensor · Square wave voltammetry · Interface modification · In situ ATRP reaction · Electroactive polymers · Poly(isopropenylphenol) · Tumor marker

Introduction

Realizing the sensitive detection of tumor markers is very urgent and momentous considering the subtle changes at different stages of cancer [1–4]. Currently, the widely recognized analytical methods for tumor marker detection include radioimmunoassay [5, 6], enzyme-linked immunosorbent assay (ELISA) [7, 8], electrochemiluminescence immunoassay (ECL) [9, 10], fluorescent immunoassay [11, 12], and other assays [13, 14]. Comparatively, electrochemical biosensors have gained precedence over the latter methods as they offer miniaturized instrumentation, rapid response, excellent sensitivity, and low cost [15–17]. However, the further development of electrochemical biosensors is limited by weak signals, signal leakage, and impaired activity of biomolecules.

To design a highly sensitive electrochemical biosensor, the signals generated from biorecognition events need to be enriched and amplified to detect trace disease biomarkers in bodily fluids [18]. At present, three common signal generation modes are carried out in electrochemical biosensors, but these still suffer from some limitations. (1) Signal substances can be attached to probes to selectively amplify the signal after recognizing targets, but the number of signal substances is limited [19–21]. (2) Signal substances can be loaded on the substrate to provide strong signals; however, they are prone to signal leakage, resulting in instability and poor repeatability [22, 23]. (3) Signal substances of high concentrations can be added into solutions to achieve strong signals, yet the biological activity of biomolecules, such as antigen, antibody, and enzymes, will be impaired [24–26]. To circumvent the above issues, it is necessary to design a high-efficiency and stable signal generation mode through constructing electrochemical biosensing interfaces.

Fei Wang and Yang Xu equally contributed to this work.

✉ Hongliang Han
hanhongliang@cnu.edu.cn

✉ Zhanfang Ma
mazhanfang@cnu.edu.cn

[1] Department of Chemistry, Capital Normal University, Beijing 100048, China

Herein, the biosensing interface was first developed based on in situ growth electrochemical signal polymers via atom transfer radical polymerization (ATRP) [27]. The target was captured by magnetic beads (MBs) modified with antibodies in tubes then labelled selectively with immunoprobes loaded with Cu(II) ions. Cu(II) ions on carbon spheres (CS) supporting immunoprobes were used as the catalyst of ATRP to facilitate polymerization. Preliminary interface modification was accomplished by fixing the initiator p-chloromethyl benzoic acid (CBA) on the amino-modifying electrode surfaces. Then, with ATRP reaction solutions (including supernatant from tubes and monomers), the poly(isopropenylphenol) (PPPL) polymer [28] with electrochemical signal in situ was generated on the electrode surfaces. Using the exceptional electroactivity of phenolic hydroxyl groups in polymers, a dramatic square wave voltammetry (SWV) signal was achieved, with a satisfyingly ultralow limit and wide detection range under optimal conditions. Moreover, the method also had a splendid detection effect on serum samples and signified outstanding potential application prospects in clinical diagnosis.

Experimental

Materials and reagents

D-(+)-glucose (99%, AR), poly(ethyleneimine) solution (PEI) (Mw = 600, GPC), sodium borohydride ($NaBH_4$) (98%, AR), and *N*-Hydroxysuccinimide (NHS) (98%, AR) were purchased from Sigma-Aldrich (Beijing, China, https://www.sigmaaldrich.com). Graphene oxide (GO) (99%, AR) was obtained from Nanjing JCNANO Tech Co. Ltd. (Nanjing, China, https://www.jcno.com). 1-(3-Dimethylaminopropyl)-3-ethylcarbodiimide hydrochloride (EDC) (98%, AR), sodium citrate (99%, AR), hydrogen tetrachloroaurate (III) trihydrate ($HAuCl_4 \cdot 3H_2O$) (99%, AR), dopamine hydrochloride (DA) (99%, AR), uric acid (UA) (99%, AR), and ascorbic acid (AA) (99%, AR) were provided from Alfa Aesar (Tianjin, China, http://www.alfa.com). 4-(Chloromethyl) benzoic acid (98%, AR) and 4-(Prop-1-en-2-yl) phenol (97%, AR) were purchased from Macklin (Shanghai, China, http://www.macklin.cn). Carboxyl-modified magnetic beads (MBs) (size = 0.4 ~ 0.5 μm, AR) were obtained from Tianjin Baselline Chrom Tech Research Centre (Tianjin, China, http://www.qiuhuan.com). Copper(II) chloride dihydrate ($CuCl_2 \cdot 2H_2O$) (98%, AR) was provided from Sinopharm Chemical Reagent Co., Ltd. (Shanghai, China, https://shreagent.lookchem.com). Carcinoma antigen 19–9 (CA19-9), CA19-9 antibody (Ab), Carcinoma antigen 12–5 (CA12-5), Carcinoma antigen 15–3 (CA15-3), Carcinoembryonic antigen (CEA), and Squamous cell carcinoma antigen (SCCA), were all provided by Shanghai Linc-Bio Science Co., Ltd. (Shanghai, China, http://www.linc-bio.com). Bovine serum albumin (BSA, standard grade) and human immunoglobulin G (IgG) were come from Beijing Xinjingke Biotechnologies Co., Ltd. (Beijing, China, http://www.bjxjk.com). Potassium ferrocyanide ($K_4Fe(CN)_6$) (97%, AR), potassium ferricyanide ($K_3Fe(CN)_6$) (98%, AR), potassium chloride (KCl) (99%, AR), and hydrochloric acid (HCl) (97%, AR) were purchased from Beijing Chemical Reagents Company (Beijing, China, www.crc-bj.com). 2,2′-Dipyridyl (BPY) (98%, AR) was provided by Aladdin Chemistry Co., Ltd. (Shanghai, China, https://www.aladdin-e.com). Human serum was supplied by Beijing GENIA Biotechnology Co. Ltd. (Beijing, China, http://e.biodee.net).

Apparatus

Transmission electron microscope (TEM) images were taken on HITACHI H7650 TEM (HITACHI, Japan, http://www.hitachi.com.cn). Scanning electron microscope (SEM) images were taken on HITACHI SU8010 SEM (HITACHI, Japan). Energy dispersive X-ray spectroscopy (EDS) was determined on HITACHI SU8010 SEM (HITACHI, Japan, http://www.hitachi.com.cn). Zeta potential measurements were performed on Zetasizer Nano ZS (Malvern Instruments Co., UK) (https://malvernchem.lookchem.com). All electrochemical measurements were carried out on CHIE660E electrochemical workstation (Chenhua Instruments Co., Shanghai, China, http://www.chinstr.com). A three electrochemical system used for all electrochemical tests was composed of a glassy carbon electrode (GCE) (4 mm in diameter) as the working electrode, a platinum wire as counter electrode, and an Ag/AgCl electrode as reference electrode.

Synthesis of poly(ethyleneimine)-graphene oxide

The poly(ethyleneimine)-graphene oxide (PEI-GO) composite was synthesized based on the previous literature [29]. GO was dispersed into deionized water at 0.1 mg mL^{-1} under continuous ultrasonic conditions. PEI solutions (10 mL, 1 mg mL^{-1}) were slowly dropped into 20 mL solution containing 0.1 mg mL^{-1} GO followed by stirring overnight to form a homogeneous system of PEI-GO. Finally, the resulting product was obtained by centrifugation and washed several times with deionized water.

Synthesis of anti-CA19-9 functionalized magnetic beads

The process of antibody modification on surfaces of magnetic beads was based on the literature [30]. Firstly, 3.0 mg carboxyl functionalized MBs were mixed with 1 mL solutions containing EDC (0.4 M) and NHS (0.1 M) and treated at 37 °C for 30 min. The MBs were collected and rinsed via magnetic separation 3 times. Then, MBs shook with 1.0 mL 200 μg ml^{-1} Ab

at 37 °C for 1 h to immobilize Ab. Finally, 1.0 mL, 1 wt% BSA was added to the mixture and stirred at 600 rpm for 30 min to seal redundant active sites. The obtained product was magnetically separated and washed 3 times by deionized water. The anti-CA19-9 functionalized magnetic beads (Ab-MBs) were dispersed in 2.0 mL deionized water and stored at 4 °C.

Synthesis of immunoprobe, anti-CA19-9 functionalized Au/Cu^{2+}/CS composites

First, the synthesis of CS as carrier according to relevant report [31]. Briefly, 4 mL 1 wt% glucose and 200 µL 10 wt% sodium citrate were mixed evenly and then reacted in microwave reaction instrument (250 W) at 160 °C for 10 min. Then, resulting mixture was centrifuged, rinsed several times, and dispersed in 2 mL deionized water. For loading of Au NPs, 10 µL of 4 wt% $HAuCl_4$ was added to the prepared CS solution and stirred for at 800 rpm for 10 min. Subsequently, 40 µL of 0.025 wt% $NaBH_4$ solution was dropped into above mixture for further 1 h. The product was collected by centrifugation at 8000 rpm for 10 min, and then redispersed in 2 mL deionized water. Finally, 1 mL 5 wt% $CuCl_2$ was added to the above suspension and stirred at 800 rpm for 1 h to adsorb Cu(II) ions. The product, Au/Cu^{2+}/CS, was collected by centrifugation at 8000 rpm for 10 min, and then redispersed in 1 mL deionized water.

Finally, for immobilization of antibodies, 100 µL, 1 mg mL^{-1} Ab was added to 1 mL solution of the above product and reacted overnight at 4 °C. To block any nonspecific binding sites, 1 mL of 1 wt% BSA was added and treated at room temperature for 1 h. The product was centrifuged at 8000 rpm for 10 min and washed by deionized water several times. The obtained Ab-Au/Cu^{2+}/CS was dispersed in 1 mL deionized water and stored at 4 °C.

Preparation of CBA-PEI-GO compound based electrochemical sensing interface

The GCE was polished with 0.05 µm alumina slurry and dried in nitrogen flow after ultrasonic washing. Fifteen-microliter PEI-GO solution was dripped onto electrode surfaces and dried. On the other hand, 1 mL mixed solution containing EDC (0.4 M) and NHS (0.1 M) was added to 1 mL CBA (3 mg mL^{-1}, DMF as solvent) and stirred at 600 rpm for 30 min to activate carboxy groups. Finally, 20 µL CBA with activated carboxyl group was dripped onto PEI-GO/GCE and incubated at 37 °C for 1 h.

Immunoreaction in tubes

First, 30 µL Ab-MBs was added to tubes. Then, 30 µL antigen samples with different concentrations (same treatment for human serum samples) were incubated with Ab-MBs at 37 °C for 50 min. Next, 30 µL immunoprobe was added and incubated at 37 °C for 40 min. After each step of immunoresponse, the immunocomplex was gathered by magnetic separation and rinsed with deionized water. To release Cu(II) ions, 10 µL HCl (1.0×10^{-4} M) was added in tubes and reacted for 10 min. Finally, 20 µL AA (3.0 mg mL^{-1}) and 10 µL BPY (0.045 mg mL^{-1}) were added to get the catalytic solution of ATRP.

Electrochemical measurement

The 10 µL monomer 4-isopropenylphenol (20 mg mL^{-1}, the volume ratio of H_2O to DMF was 1:1 as solvent) and 10 µL catalytic solution was dripped onto CBA-PEI-GO/GCE and treated at 37 °C for 1 h. Finally, square wave voltammetry (SWV) was conducted from 0 to 0.9 V in 10 mM phosphate buffer containing 0.1 M KCl (pH = 7.4) to read out the electrochemical signal after rinsing with deionized water.

Results and discussion

Principle of designed biosensing interface

The main steps and principles of the biosensing interface are shown in Scheme 1, including the immune recognition in tubes and the construction of electrochemical biosensing interfaces (as shown in part A). On the one hand, the immune recognition adopted the sandwich structure in tubes, whereby magnetic separation enabled the separation and enrichment of targets. The anti-CA19-9 functionalized Au/Cu^{2+}/CS composites (Ab-Au/Cu^{2+}/CS NPs) immunoprobes were designed using Cu(II) ions as the catalyst, CS as the carrier connected antibodies to Au NPs, and adsorbed Cu(II) ions via electrostatic interaction. On the other hand, the biosensing interface was constructed based on ATRP in situ growth signal polymers, PPPL, with electrochemical activities. The initiator CBA was first fixed by PEI-GO with rich amino groups to accomplish the preliminary modification of electrode surfaces via carbodiimide/succinimide chemistry (Fig. S3). Subsequently, the catalyst Cu(II) ions released from immunoprobes through acid stimulation were converted into Cu(I) ions by AA, then PPPL in situ ATRP polymerized generated with the complexing agent BPY and the monomer 4-isopropylphenol on modified electrode interfaces (as shown in part B) (Fig. S4) [32, 33]. With the increment of Cu(II) ions as the catalyst, the phenolic hydroxyl groups attached to the polymerized long-chain increased. As a result, the sensitive detection of CA19-9 was achieved successfully, taking advantage of the inherent amplification in the chain-growth process, based on increasing the number of electroactive signal tags.

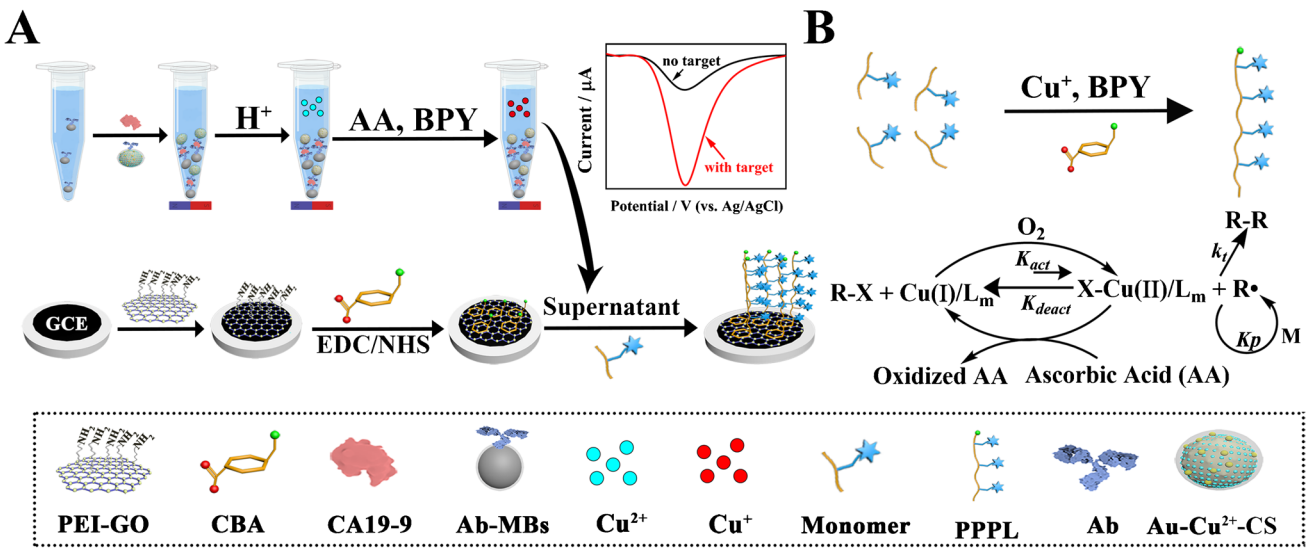

Scheme 1 Schematic illustrations of in situ grown electroactive polymers via ATRP to construct biosensing interface

Characterization of immune-recognition part: Au/Cu^{2+}/CS probes

To explore the changes in surface charges of the immune probe formation process, the zeta potential was monitored by an electrophoretic light scattering technique (Fig. 1). The zeta potentials of CS and Au/CS were measured to be − 23.5 (Fig. 1A) and − 29.3 mV (Fig. 1B), respectively, and increased to − 4.1 mV (Fig. 1C) after introducing Cu(II) ions, indicating that a large amount of Cu(II) ions were successfully adsorbed onto the immunoprobe by electrostatic force. Moreover, the pH of HCl changed from 4.0 to 4.6 after treatment of immunocomplex, revealing H^+ ions absorbed to the CS and Cu(II) ions unlocked into acid solution via ion exchange between H^+ and Cu^{2+} [34], demonstrating the successful release of Cu(II) ions. As shown in Fig. 2A, the morphology of CS as the basic carrier was identified by TEM. The TEM images reveal that CS exhibits a uniform nanosphere structure with an average diameter of about 200 nm and a slightly uneven surface with a large specific surface area. Following the in situ growth of Au NPs, a large number of small black spots (with an average diameter of about 10 nm) could be observed on the surface of CS (Fig. S1A). In addition, it was confirmed as Au NPs by EDS, C, O, and Au, proving Au NPs were loaded on CS (Fig. S1B). Finally, Cu(II) ions were loaded onto Au/CS via electrostatic attraction. As shown in Fig. 2B, there was no obvious change on the surface of probes, because Cu(II) ions were too small to be observed. The presence of Cu(II) ions was further determined by EDS (Fig. 2D), which also revealed the presence C, O, Cu, and Au elements, as expected.

Characterization of biosensing interface part: PEI-GO, CBA-PEI-GO, and the PPPL

The biosensing interface was constructed into three layers, which were constructed by a drip coating method. The first layer was the aminated electrode surface using amino-rich polymer-modified GO (PEI-GO) nanosheets which could be observed by SEM (Fig. 3A). The characteristic elements of PEI-GO were confirmed by EDS (Fig. 3C), where C and O came from GO, and N from -NH_2 groups of PEI, proving the successful modification of the first layer (the Au element was produced via EDS testing). Then, the second layer was initiator CBA, which connected carboxyl groups with the modified amino groups on the electrode surfaces

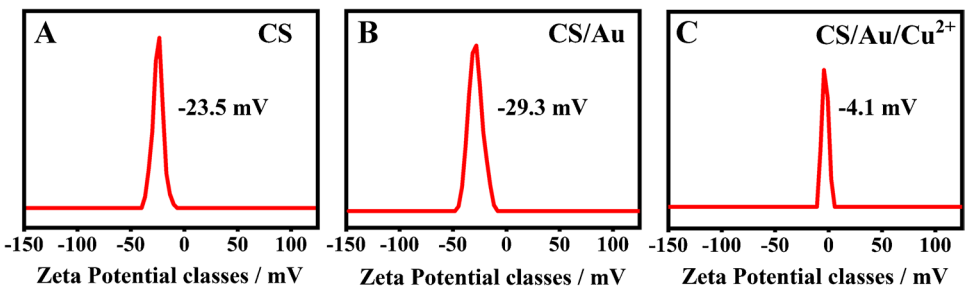

Fig. 1 Zeta value changes during formation of immunoprobes: CS (**A**), CS/Au (**B**), and CS/Au/Cu^{2+} (**C**)

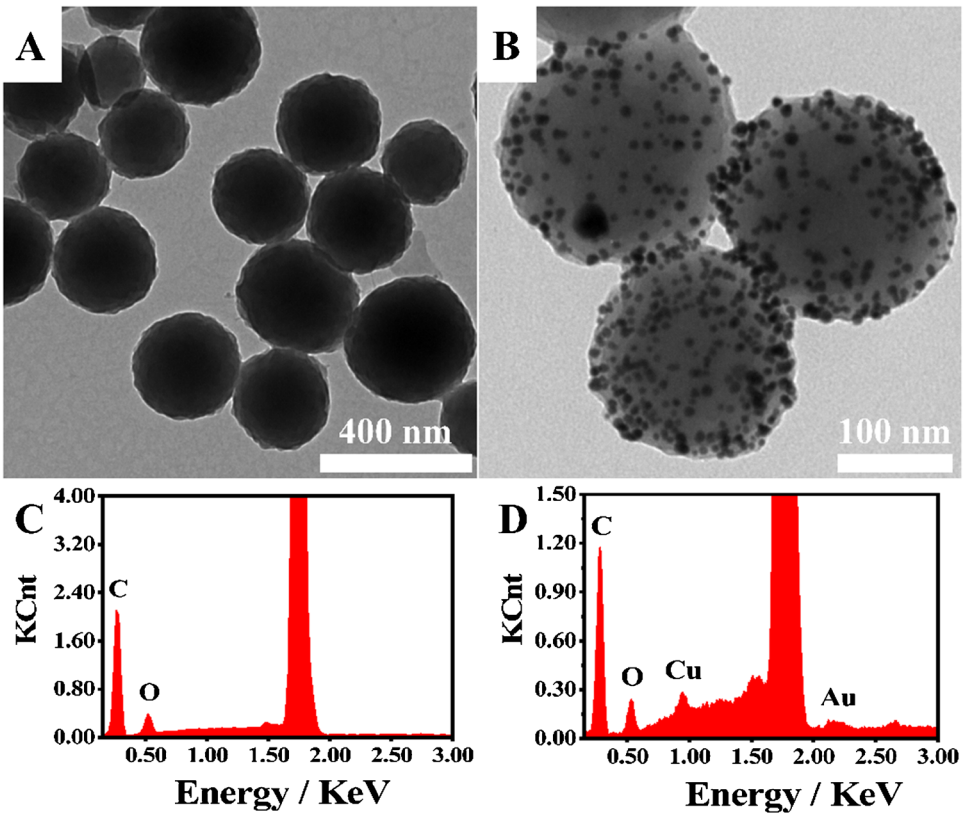

Fig. 2 TEM images of CS (**A**), and Au/Cu^{2+}/CS (**B**). EDS spectra of CS (**C**), and Au/Cu^{2+}/CS (**D**)

by EDC/NHS. Results reveal the smoother surface of the electrode (Fig. 3B), whereby characteristic element Cl was attributed to CBA (Fig. 3D). The third layer contained the long polymer PPPL in situ chains with the electrochemical signal. Figure 3E and F indicate the widespread distribution of linear polymer chains that formed in situ on the initiator functionalized PEI-GO nanosheets.

Electrochemical characterization of biosensor construction

To verify the feasibility of biosensing interfaces, the electrical signals of each process to construct biosensing interface were detected by SWV (Fig. 4A). As expected, no obvious electric signal was generated at an early stage then expanded rapidly after electroactive polymer was formed. This provides strong support for the detection of relevant biomolecules.

The layer-by-layer modification process of the electrode surface was monitored by electrochemical impedance spectroscopy (EIS) in 10 mM phosphate buffer containing 0.1 M KCl and 5 mM $[Fe(CN)_6]^{4-/3-}$. As shown in Nenquist plots, the modification of different materials directly affected interfacial properties, including the magnitude of charge transfer resistance (R_{ct}) and change in the semicircle diameter. According to the results shown in Fig. 4B, the semicircle diameter goes from small to large as PEI-GO, CBA-PEI-GO, bare GCE, PPPL-PEI-GO. Specifically, PEI-GO with excellent conductivity obtained the smallest semicircle. After connecting CBA, interfacial resistance increased as predicted, and the semicircle increased to a size similar to that of a bare electrode. Finally, the growth of long polymer chains further increased the interfacial resistance and achieved the largest semicircle. Each modification procedure is consistent with the results of EIS, confirming the successful construction of biosensing interfaces. However, it was exactly due to the poor conductivity of PPPL that the output current was small, which limited the further development of this sensor.

Optimization

To obtain the best detection effect of the electrochemical biosensing interfaces, three influencing factors were investigated, including pH of Cu(II) ions release, the concentration of CBA, and incubation time of immunoprobes. It could be concluded from Fig. S2A the optimal concentration of CBA was 3 mg mL^{-1}. At lower concentrations, as the number of initiators increased, the number of polymerized long chains increased, and the electrical signal became stronger. However, a high initiator density may lead to an increase in chain transfer or chain termination, which can delay the polymer growth and decrease the electrical signal. In addition, pH showed to affect the

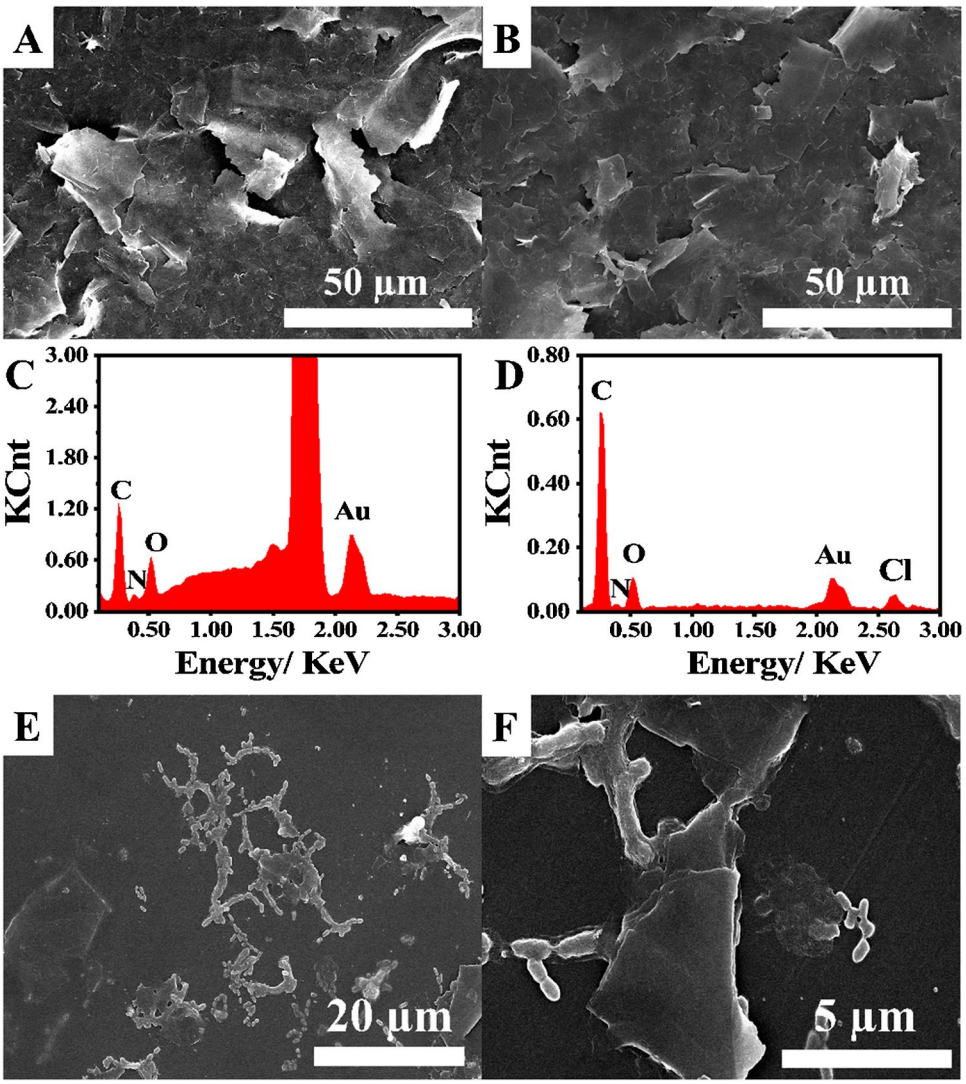

Fig. 3 SEM images of PEI-GO (**A**) and CBA-PEI-GO (**B**). EDS spectra of PEI-GO (**C**), and CBA-PEI-GO (**D**). SEM images of PPPL (**E**, **F**)

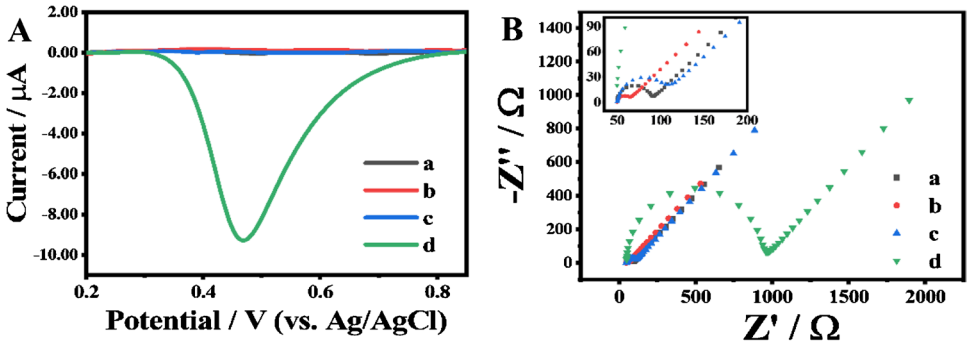

Fig. 4 SWV (**A**) in 0.01 M phosphate buffered solution containing 0.1 M KCl solution and EIS (**B**) in 0.01 M phosphate buffered solution containing 5 mM $[Fe(CN)_6]^{4-/3-}$ 0.1 M KCl of different modified electrodes: GCE (a), PEI-GO/GCE (b), CBA-PEI-GO/GCE (c), and PPPL-PEI-GO/GCE (d)

release of Cu(II) ions and the acidic environment in which polymerization took place. Although more Cu(II) ions were released at a lower pH, an over-acidic environment would reduce the activity of the polymerization reaction; there a pH of 4.0 was determined as the optimal value for the best electrical signal (Fig. S2C). As shown in Fig. S2B, the electrical signal did not increase significantly after 40 min; thus, the optimal incubation time as the third factor was determined to be 40 min.

Analytical performance of the biosensor

After defining the optimal detection conditions of the biosensor, the quantitative relationship between target

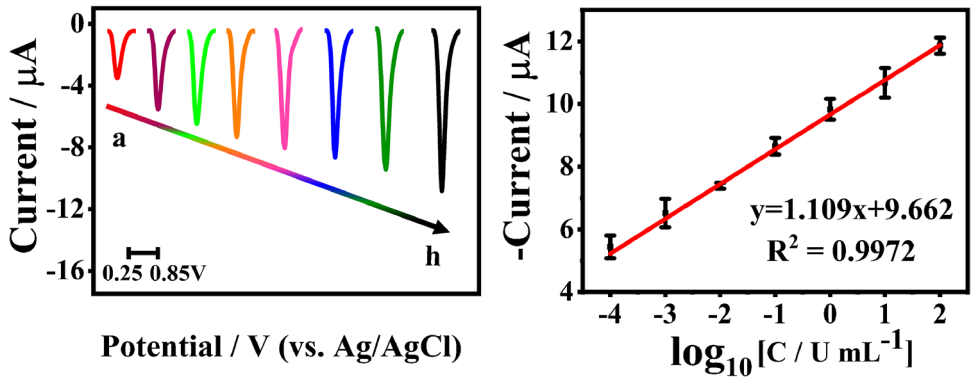

Fig. 5 **A** SWV responses of electrochemical detection for CA19-9 in 0.01 M phosphate buffered solution containing 5.0 mM $[Fe(CN)_6]^{4-/3-}$ and 0.1 M KCl (pH 7.4) at the concentrations from 0.0001 to 100 U mL^{-1} (line a was 0 U mL^{-1} and line b to h meant 0.0001 to 100 U mL^{-1}). **B** The calibration plot between the SWV peak current (0.22 V vs. Ag/AgCl) and the logarithm values of CA19-9 concentrations (the error bars are standard deviations for $n = 3$)

Table 1 Comparison of the recently reported immunoassay for detection of CA19-9

Method	Linear range (U mL^{-1})	Detection limit (U mL^{-1})	Ref
Fluorescent	0.1–1000	0.09	[37]
Fluorescent	1.0–10	0.36	[38]
Chemiluminescence	0.5–20	0.20	[39]
Electrochemical	1.0×10^{-3}–200	1.63×10^{-4}	[40]
Electrochemical	2.1×10^{-13}–200	2.10×10^{-13}	[41]
Electrochemical	1.0×10^{-4}–100	3.90×10^{-5}	This work

CA19-9 concentrations and detection signal values (current responses about SWV measurements) was studied (Fig. 5A, B). It could be observed that from 0.0001 to 100 U mL^{-1}, current signals increased with increasing concentration, which was expected. A clear linear relationship was further established: $-I = 1.109\log_{10}C_{CA19\text{-}9} + 9.662$, $R^2 = 0.9972$, which is exhibited in the calibration plot of the current response differences and CA19-9 concentration. Moreover, the detection limit of the sensor was 0.039 mU mL^{-1} at a signal-to-noise ratio of 3σ ($S/N = 3$) (σ is the standard deviation of signal in a black solution) [35, 36]. Compared with the previously reported biosensor, our proposed sensor broadens the detection range and greatly reduces the detection limit (Table 1).

Specificity, precision, and stability of the biosensing interface

To maintain excellent detection performance in complex environments, specificity of the proposed biosensor was investigated by adding interference substances (Fig. 6A), such as ascorbic acid (AA), dopamine hydrochloride (DA), uric acid (UA), immunoglobulin G (IgG), squamous cell

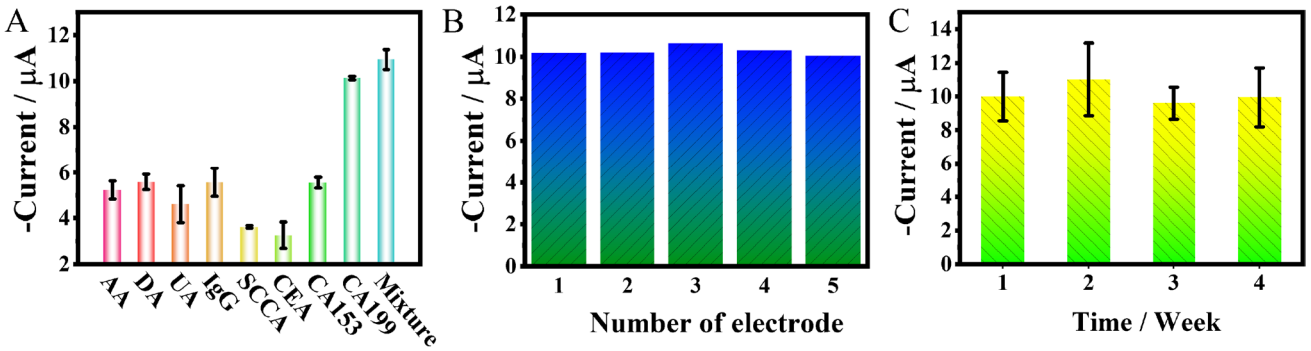

Fig. 6 The specificity of the biosensor for AA (100 ng mL^{-1}), DA (100 ng mL^{-1}), UA (100 ng mL^{-1}), IgG (100 ng mL^{-1}), SCCA (100 ng mL^{-1}), CEA (100 ng mL^{-1}), CA15-3 (100 U mL^{-1}), CA19-9 (10 U mL^{-1}), and mixture (**A**). Precision of 5 different electrodes for detection of 10 U mL^{-1} of CA19-9 (**B**). SWV current responses about stability of the biosensing interface for 4 weeks (**C**). The error bars are standard deviations ($n = 3$)

carcinoma antigen (SCCA), carcinoembryonic antigen (CEA), and carcinoma antigen 15–3 (CA15-3). Results show that the effect of distractions was negligible and the high response currents of CA19-9 and signal were retained, thus confirming high specificity. To guarantee repeatability of detection performance, five different biosensing interfaces were constructed to detect CA19-9 (Fig. 6B). The relative standard deviation (*RSD*) was found to be less than 5%, indicating excellent precision. Subsequently, the stability of the biosensor was tested at 4 °C for 4 weeks. Results show that the relative standard deviation was less than 10%, therefore confirming good stability of the analysis interface (Fig. 6C).

Practical application of the biosensing interface

To ensure accuracy and reliability of the designed biosensor in actual sample detection, human serum samples were analyzed, and results were compared with the standard electrochemiluminescence method. Detection results showed that this biosensor had achieved satisfying performance in human blood serum with good inter-assay precision ($RSD < 6\%$) and satisfactory recovery of ~ 99–105%, suggesting the practicability of this method in actual serum detection (Table S1).

Conclusion

In this work, a simple biosensing interface was developed based on ATRP in situ growth signal polymers to achieve the sensitive detection of CA19-9. PPPL polymer was directly used as the signal substance considering its inherent electrochemical activity, which can provide sufficient signals for the biosensor, avoid signal leakage and streamline the interface modification. Overall, this work provides a novel method to construct high-effective biosensing interfaces, improving the practical application ability of polymerization-based biosensors for relevant biomolecular detection.

Supplementary Information The online version contains supplementary material available at https://doi.org/10.1007/s00604-021-05048-w.

Funding This research was financed by grants from Joint project of Beijing Municipal Education Commission and Beijing Natural Science Foundation (KZ202110028042), National Natural Science Foundation of China (22172104, 21673143), and Capacity Building for Sci-Tech Innovation-Fundamental Scientific Research Funds (20530290087, 20530290055).

References

1. Siegel RL, Miller KD, Jemal A (2019) Cancer statistics, 2019. CA Cancer J Clin 69:7–34
2. Ferlay J, Colombet M, Soerjomataram I et al (2019) Estimating the global cancer incidence and mortality in 2018: globocan sources and methods. Int J Cancer 144:1941–1953
3. Karley D, Gupta D, Tiwari A (2011) Biomarker for cancer: a great promise for future. World J Oncol 2:151–157
4. Rabinowits G, Gerçel-Taylor C, Day JM et al (2009) Exosomal microRNA: a diagnostic marker for lung cancer. Clin Lung Cancer 10:42–46
5. Del Villano BC, Brennan S, Brock P et al (1983) Radloimmunometric assay for a monoclonal antibody-defined tumor marker, CA 19–9. Clin Chem 29:549–552
6. Kaur S, Smith LM, Patel A et al (2017) A combination of MUC5AC and CA19-9 improves the diagnosis of pancreatic cancer: a multicenter study. Am J Gastroenterol 112:172–183
7. Lequin RM (2005) Enzyme immunoassay (EIA)/enzyme-linked immunosorbent assay (ELISA). Clin Chem 51:2415–2418
8. Heidari MH, Porghasem M, Mirzaei N et al (2014) The effect of high level natural ionizing radiation on expression of PSA, CA19-9 and CEA tumor markers in blood serum of inhabitants of Ramsar. Iran J Environ Radioact 128:64–67
9. Babamiri B, Hallaj R, Salimi A et al (2017) Potential-resolved electrochemiluminescence immunoassay for simultaneous determination of CEA and AFP tumor markers using dendritic nanoclusters and Fe_3O_4@SiO_2 nanoparticles. Microchim Acta 184:3613–3623
10. Chen D, Zhang M, Zhou F et al (2019) Ultrasensitive electroluminescence biosensor for a breast cancer marker microRNA based on target cyclic regeneration and multi-labeled magnetized nanoparticles. Microchim Acta 186:628
11. Chen H, Luo D, Shang B et al (2020) Immunoassay-type biosensor based on magnetic nanoparticle capture and the fluorescence signal formed by horseradish peroxidase catalysis for tumor-related exosome determination. Microchim Acta 187:282
12. Wang J, Liu H, Huang X, Ren J (2015) Homogeneous immunoassay for the cancer marker alpha-fetoprotein using single wavelength excitation fluorescence cross-correlation spectroscopy and CdSe/ZnS quantum dots and fluorescent dyes as labels. Microchim Acta 183:749–755
13. Olmsted IR, Hassanein M, Kussrow A et al (2014) Toward rapid, high-sensitivity, volume-constrained biomarker quantification and validation using backscattering interferometry. Anal Chem 86:7566–7574
14. Lu N, Gao A, Dai P et al (2015) Ultrasensitive detection of dual cancer biomarkers with integrated CMOS-compatible nanowire arrays. Anal Chem 87:11203–11208
15. Ibáñez-Redín G, Materon EM, Furuta RHM et al (2020) Screen-printed electrodes modified with carbon black and polyelectrolyte films for determination of cancer marker carbohydrate antigen 19–9. Microchim Acta 187:417
16. Gao Y, Huo W, Zhang L et al (2019) Multiplex measurement of twelve tumor markers using a GMR multi-biomarker immunoassay biosensor. Biosens Bioelectron 123:204–210
17. Putnin T, Ngamaroonchote A, Wiriyakun N et al (2019) Dually functional polyethylenimine-coated gold nanoparticles: a versatile material for electrode modification and highly sensitive simultaneous determination of four tumor markers. Microchim Acta 186:305
18. Guo K, Wustoni S, Koklu A et al (2021) Rapid single-molecule detection of COVID-19 and MERS antigens via nanobody-functionalized organic electrochemical transistors. Nat Biomed Eng. https://doi.org/10.1038/s41551-021-00734-9
19. Zhang DS, Li WX, Wang HQ, Ma ZF (2018) A novel immunoprobe composed of reduced graphene oxide-hemin-thionin-Au nanohybrid for ultrasensitive detection of tumor marker. Sens Actuators B: Chem 258:141–147

20. Shen WJ, Zhuo Y, Chai YQ et al (2015) Enzyme-free electrochemical immunosensor based on host-guest nanonets catalyzing amplification for procalcitonin detection. ACS Appl Mater Interfaces 7:4127–4134
21. Chen Y, Wang AJ, Yuan PX et al (2019) Three dimensional sea-urchin-like PdAuCu nanocrystals/ferrocene-grafted-polylysine as an efficient probe to amplify the electrochemical signals for ultrasensitive immunoassay of carcinoembryonic antigen. Biosens Bioelectron 132:294–301
22. Huang ZJ, Jiang ZQ, Zhao CF et al (2017) Simple and effective label-free electrochemical immunoassay for carbohydrate antigen 19–9 based on polythionine-Au composites as enhanced sensing signals for detecting different clinical samples. Int J Nanomedicine 12:3049–3058
23. Meng XZ, Xu Y, Zhang NN et al (2021) Ferric hydroxide nanocage triggered Fenton-like reaction to improve amperometric immunosensor. Sens Actuators B: Chem 338:129840
24. Cai XH, Weng SH, Guo RB et al (2016) Ratiometric electrochemical immunoassay based on internal reference value for reproducible and sensitive detection of tumor marker. Biosens Bioelectron 81:173–180
25. Li LD, Zhao HT, Chen ZB et al (2011) Aptamer biosensor for label-free square-wave voltammetry detection of angiogenin. Biosens Bioelectron 30:261–266
26. Deng CY, Qu FL, Sun HY, Yang M et al (2011) Sensitive electrochemical immunosensor based on enlarged and surface charged gold nanoparticles mediated electron transfer. Sens Actuators B: Chem 160:471–474
27. Kim S, Sikes HD (2020) Radical polymerization reactions for amplified biodetection signals. Polym Chem 11:1424–1444
28. Ito H, Willson CG, Frechet JMJ (1983) Synthesis of poly(p-hydroxy-a-methylstyrene) by cationic polymerization and chemical modification. Macromolecules 16:510–517
29. Choi HY, Lee TJ, Yang GW et al (2017) Generation of integration-free induced neurons using graphene oxide-polyethylenimine. Small 13:1601993
30. Zheng Y, Ma ZF (2019) Multifunctionalized ZIFs nanoprobe-initiated tandem reaction for signal amplified electrochemical immunoassay of carbohydrate antigen 24–2. Biosens Bioelectron 129:42–49
31. Choma J, Jamiola D, Augustynek K et al (2012) Carbon-gold core-shell structures: formation of shells consisting of gold nanoparticles. Chem Commun (Camb) 48:3972–3974
32. Qian H, He L (2009) Detection of protein binding using activator generated by electron transfer for atom transfer radical polymerization. Anal Chem 81:9824–9827
33. Qian H, He L (2009) Surface-initiated activators generated by electron transfer for atom transfer radical polymerization in detection of DNA point mutation. Anal Chem 81:4536–4542
34. Zhao HW, Yang GP, Hill AJ et al (2021) One-step ion-exchange from Na-SSZ-13 to Cu-SSZ-13 for NH_3-SCR by adjusting the pH value of Cu-exchange solution: The effect of H^+ ions on activity and hydrothermal stability. Microporous Mesoporous Mater 324:111271
35. Loock HP, Wentzell PD (2012) Detection limits of chemical sensors: applications and misapplications. Sens Actuators B: Chem 173:157–163
36. Montville D, Voigtman E (2003) Statistical properties of limit of detection test statistics. Talanta 59:461–476
37. Jiao YC, Du C, Zong LJ et al (2020) 3D vertical-flow paper-based device for simultaneous detection of multiple cancer biomarkers by fluorescent immunoassay. Sens Actuators B: Chem 306:127239
38. Gan N, Xie LS, Zhang K et al (2018) An endonuclease-linked multiplex immunoassay for tumor markers detection based on microfluidic chip electrophoresis for DNA analysis. Sens Actuators B: Chem 272:526–533
39. Chu W, Chen Y, Liu W et al (2017) Paper-based chemiluminescence immunodevice with temporal controls of reagent transport technique. Sens Actuators B: Chem 250:324–332
40. Kalyani T, Sangili A, Nanda A et al (2021) Bio-nanocomposite based highly sensitive and label-free electrochemical immunosensor for endometriosis diagnostics application. Bioelectrochemistry 139:107740
41. Staden RS, Gheorghe SS, Ilie-Mihai RM et al (2021) Disposable stochastic sensor based on deposition of a nanolayer of silver on silk for molecular recognition of specific biomarkers. J Electrochem Soc 168:037515